Journal of Solid State Chemistry 182 (2009) 602–607

Contents lists available at ScienceDirect

Journal of Solid State Chemistry

journal homepage: www.elsevier.com/locate/jssc

Hydrogen activated axial inter-conversion in SiC nanowires

Mark H. Rümmeli [a,*], David B. Adebimpe [b], Ewa Borowiak-Palen [c], Thomas Gemming [a], Paola Ayala [d], Nicholas Ioannides [e], Thomas Pichler [f], Andrzej Huczko [g], Stanisław Cudziło [h], Martin Knupfer [a], Bernd Büchner [a]

[a] IFW Dresden, P.O. Box 270116, D-01171 Dresden, Germany
[b] Polymath Interscience LLC, 3 Church Circle, Suite 366, Annapolis, MD 21401, USA
[c] Szczecin University of Technology, KnowMatTec, Szczecin, Poland
[d] Laboratory of Physics and Center for New Materials, Helsinki University of Technology, P.O. Box 5100, 02150 Espoo, Finland
[e] London Metropolitan University, 166-220 Holloway Road, London, UK
[f] Department of Physics, Vienna University, Strudlhofgasse 4, A-1090 Wien, Austria
[g] Department of Chemistry, Warsaw University, Pasteura 1, Warszawa 02-093, Poland
[h] Military University of Technology (WAT), Kaliskiego 2, Warszawa 00-908, Poland

ARTICLE INFO

Article history:
Received 11 August 2008
Received in revised form
30 October 2008
Accepted 14 December 2008
Available online 24 December 2008

Keywords:
Silicon carbide
Nanowires
Nanotubes
Hydrogen
Activation

ABSTRACT

A facile low pressure annealing route using NH_3 as a hydrogen source for the structural and chemical modification of SiC nanowires (SiCNWs) is presented. The developed route transforms SiCNWs into tubular SiC nanostructures while coaxial SiO_2/SiCNWs reverse their sheath/core structure. Our findings suggest a decomposition process induced via the preferential substitution of silicon by hydrogen and via the difference in diffusion rates of available atomic species, which leads to axial structural rearrangement. In addition to these effects, the procedure improves the crystallinity of the samples. The process could be exploited as a viable route to manipulate a variety of nanostructures and films for doping and etching and structural manipulation.

1. Introduction

SiC is a most-important material for a variety of applications. Its properties include high mechanical strength, high thermal stability and thermal conductivity, chemical inertness, a large band gap [1,2] and strong resistance to high doses of radiation [3]. In terms of material applicability stemming from its outstanding properties, it represents a basic ingredient for metal-oxide-semiconductor (MOS) devices. Due to these attractive properties, the semiconductor industry has always viewed SiC as a realistic contender to replace Si, which suffers from sensitivity to heat. Until recently, flaws known as micropipes plagued SiC single crystal formation. However, Japanese workers claim to have now overcome these structural defects [4] and are able to synthesize wafers that are "virtually dislocation-free." This makes SiC a superior contender for silicon's applications. In addition to usurping the electronic characteristics of silicon, the very good thermal and mechanical characteristics of SiC also makes it attractive as a key component in composite-material fabrication. For example, SiC is used as a coating material in the nose cone of the space shuttle to protect the carbon–carbon composites from oxidation in the high temperature air environments it has to withstand upon re-entry into the earth's atmosphere [5]. Also, silicon carbide fiber reinforced silicon carbide matrix composites are attractive materials for use in gas turbine hot sections [6] and in the fabrication of high-performance disc brakes where Si reacts with the carbon forming thermally stable SiC. The current interest in the quantum properties of one-dimensional (1D) nanomaterials such as nanotubes and nanowires, for both fundamental studies and applications in nanoscale electronic or optoelectronic devices, also applies to SiC based nanostructures. SiC nanostructures have exhibited superior optical and field electron emission properties than bulk SiC [7]. In effect, there is an ever-growing interest in the synthesis of SiC nanospheres, nanotubes and nanowires as functional materials [8]. Although various techniques exist to synthesize SiC nanowires (SiCNWs) [9,10] and nanotubes [11,12], few, if any, studies exist on routes through which to manipulate 1D SiC nano-systems. In this contribution we present a low pressure (5×10^{-5} mbar) hydrogen (from decomposed NH_3) activated thermal route to manipulate and restructure 1D SiC nano-systems. Furthermore, we demonstrate how the developed route can convert SiCNW into tubular SiC nanostructures, and

* Corresponding author. Fax: +49 351 4659 440.
E-mail address: m.ruemmeli@ifw-dresden.de (M.H. Rümmeli).

0022-4596/$ - see front matter © 2008 Elsevier Inc. All rights reserved.
doi:10.1016/j.jssc.2008.12.004

how the route is also applied to hetero SiCNWs. In our study, coaxial SiCNWs with an SiO_2 cladding were inter-converted to SiO_2 nanowires clad in SiC. The ability to manipulate these SiC nano-systems will enable new and interesting possibilities.

2. Experimental details

The as made SiCNWs where produced in a thermal treatment process from bundles of single walled carbon nanotubes in the presence of Si, using published methods [12]. The coaxial SiO_2/SiCNWs were produced by combustion synthesis of mixtures containing Si-containing compounds and halocarbons (Si and polytetrafluoroethylene, PTFE—ratio 36:64) in a calorimetric bomb [9].

The hydrogen activated modification of the SiC nanostructures was accomplished by placing the starting material in an Al_2O_3 crucible placed at the center of a horizontal tube furnace (Carbolite STF 16/180). Prior to the reaction the reactor was evacuated to base pressures better than 10^{-7} mbar. After evacuation the oven was heated up to a temperature of 1450 °C. Once the desired temperature had been reached, NH_3 or N_2 was released into the reaction chamber via a highly sensitive needle valve to a pressure of 5×10^{-5} mbar. *Note*: NH_3 at low pressure begins to decompose around 500 °C and so serves as a hydrogen source in these experiments. Various dwell times were explored. The morphology of the nanostructures were studied using scanning electron microscopy (SEM, Hitachi S4500) and transmission electron microscopy (TEM, FEI Tecnai F30, 300 kV) which also allowed spatial local electron energy loss spectroscopy (EELS) line scans to be conducted in the scanning TEM (STEM) mode. Additional bulk EELS measurements were conducted in a purpose built high-resolution spectrometer [13] where the energy resolution was set to 200 meV and the momentum resolution was 0.1 $Å^{-1}$. IR optical absorption spectroscopy was measured using a Bruker 113 Fourier transform spectrometer with a resolution of 0.5 cm^{-1}, while Raman spectra were obtained using a Bruker FT Raman spectrometer (1064 nm) with a resolution of 2 cm^{-1}.

3. Results and discussion

Fig. 1a and b show SEM images of the starting SiCNW material at low and high magnifications, respectively. TEM studies confirmed the presence of both SiCNWs with both uniform and non-uniform widths (Fig. 1) and determined the nanowire diameters to range between 20 and 100 nm. The TEM studies also showed the crystalline nature of the nanowires (e.g. Fig. 1e inset). Bright field TEM studies (e.g. Fig. 1c) and the high angle annular dark field (HAADF) studies (e.g. Fig. 1d) showed the nanowires to contain many stacking faults. Bragg diffraction studies showed the samples to be a mixture of SiC α and β phases with random orientation. These stacking faults are typical of SiCNWs [14,15] and are a result of the many polytypes (over 100) that exist in SiC.

The vibrational properties of the samples were analyzed by Raman and IR spectroscopy. The Raman spectrum (Fig. 2 left panel, lower spectrum), shows a broad asymmetric peak with a maximum around 940 cm^{-1} and a broad shoulder at lower wavenumbers. The peak at ca. 940 cm^{-1} corresponds to longitudinal optical (LO) modes and is the strongest of the SiC modes [16]. A weaker transverse optical (TO) mode, usually present in SiC just below 800 cm^{-1}, is not too apparent in the spectrum. This mode is highly dependent on the excitation energy [17], which may, in part, account for it not being clearly observable with the SiCNW sample. The large width, asymmetry, and the shoulder of

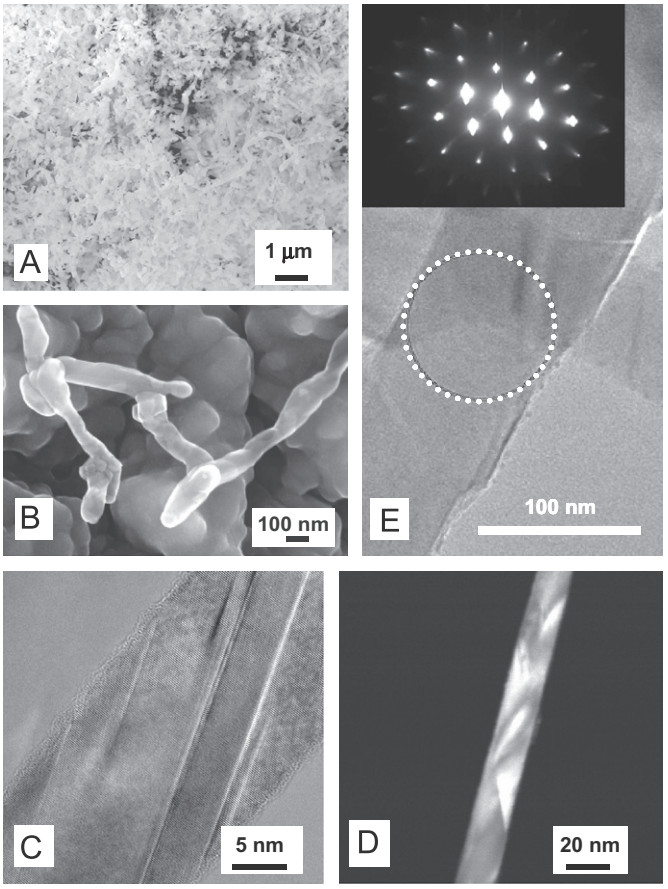

Fig. 1. (A, B) SEM micrographs of SiC nanowires. (C) Bright field TEM microgram of SiC nanowire. Stacking faults are clearly visible. (D) HAADF micrograph of SiC nanowire showing stacking faults. (E) TEM image of nanowire. *Inset*: diffraction pattern (2H polytype) from circled region.

the observed Raman response arise from a variety of rationale. The TO and LO lines broaden and shift due to lattice imperfections. In addition, phonon modes vary slightly between each polytype and so a sample composed of multiple polytypes will yield a broad response [18]. Furthermore, finite size effects can also broaden the responses. In this latter instance, force constants are reduced, leading to a red shift in the Raman response. The size distribution exhibited by these nanostructures will lead to red shifts and a frequency distribution which results in a broad and asymmetric Raman response. However, if size effects were a key effect we might also expect the post-treated Raman spectrum to be up-shifted relative to the starting spectrum. Since this is not observed, this suggests that polytype changes and lattice imperfections are also at play. Fig. 2, right panel (lower spectrum) shows the IR response from the starting SiCNW material. The features between 700 and 1000 cm^{-1} arise from the same phonon mode, which is susceptible to LO–TO splitting. The more pronounced peak at 796 cm^{-1} corresponds to the transverse mode of the optical phonon (TO) whilst the shoulder at 930 cm^{-1} corresponds to the longitudinal mode of the optical phonon (LO). While local studies of the starting sample, using scanning TEM (STEM) based EELS, show the nanowires to be composed entirely of SiC, EELS line scans across the nanostructures reveal the presence of two types of SiCNWs. The majority of the species present are considered to be solid SiCNW. An example of such a nanowire is shown in Scheme 1a where parabolic C and Si profiles, corresponding to a solid nanowire, are observed from the EELS line scan. A few of the nanowires, however, exhibit flatter C and Si profiles as illustrated in Scheme 1b. This we attribute to the

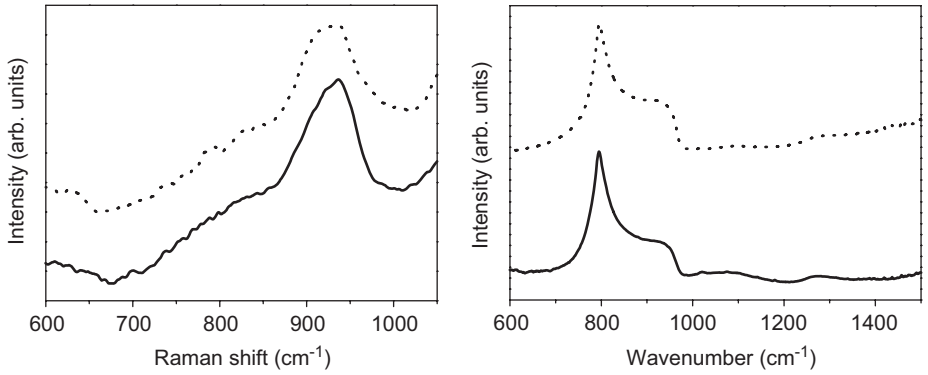

Fig. 2. Vibrational spectra of starting and post-treated samples. *Left panel*: Raman spectra of starting SiCNW (full curve) and treated SiCNW (dotted curve). *Right panel*: IR absorption spectra of starting SiCNW (full curve) and treated SiCNW (dotted curve).

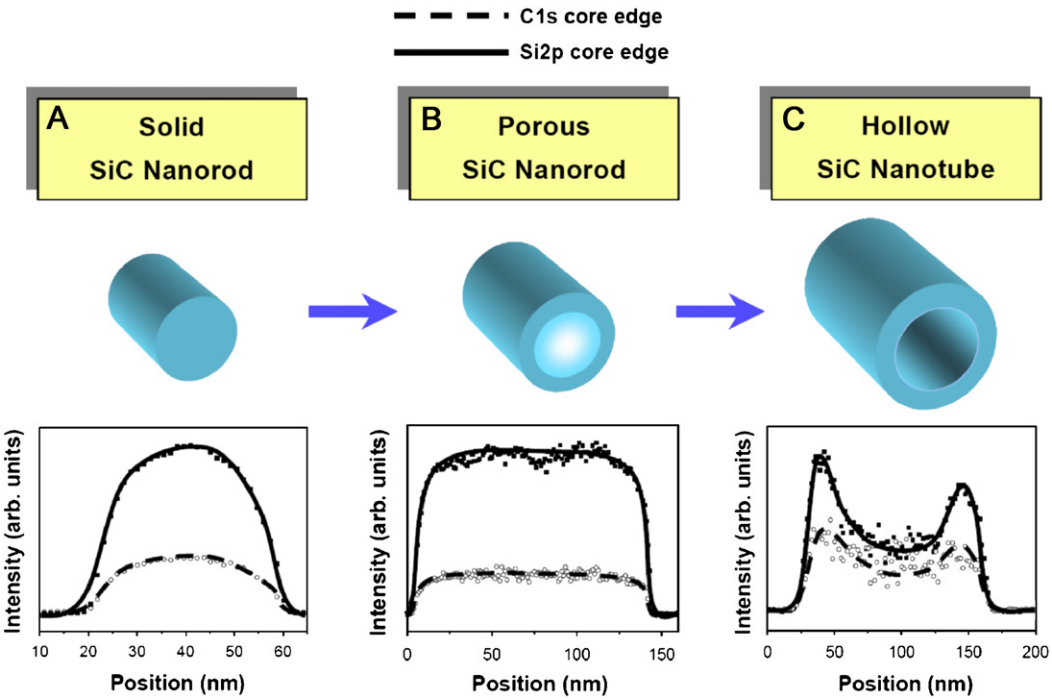

Scheme 1. The progressive conversion of (A) SiCNW, through (B) porous SiCNW, to (C) SiC nanotube, with hydrogen treatment. Lower panels show STEM based EELS line scans across each of the SiC nanostructures for the C1*s* and Si2*p* edges. Notice the diameter increase as material conversion progresses from a nanorod to a nanotube.

SiCNW being porous. Hence this starting material can be considered composed primarily of SiCNW ($>90\%$) and a diminutive amount of porous SiCNW.

The starting SiCNW material was annealed in ammonia (5×10^{-5} mbar) at 1450°C for 3 h and again subjected to physico-chemical characterization. Bragg diffraction studies showed no change in the crystalline nature of the sample, viz. a mix of SiC α and β phases with random orientation. In addition, the Raman and IR spectra (Fig. 2 left and right panels, respectively) showed no significant change. However, the Raman spectra did now show a weak peak at ca. 796 cm^{-1} corresponding to the SiC TO mode. This can be attributed to fewer lattice imperfections being present in the sample. However, TEM studies revealed that the material had undergone substantial morphological changes. TEM bright field observations show that the sample still consists of nanowires; however, local EELS line scans across the nanowires showed that most of the resultant SiCNW were now hollow (Scheme 1c), as typical Si and C profiles for these structures now dip to a minimum around the center due to their hollow nature. In effect, the structures are SiC nanotubes. Of the remaining structures most were porous SiCNW and a diminutive number of SiCNW were also present (Scheme 1b and a, respectively). In addition to these changes, the diameters of the structures had also increased, now ranging from 40 to 250 nm. The diameters for the engendered SiC nanotubes (70%) were the largest, followed by the porous nanowires (25%) and the solid nanowires (5%) had the smallest diameters. This might suggest SiCNW progressively convert to porous SiCNW and then hollow SiCNW (tubular SiC nanostructures).

Morphological changes induced by the ammonia treatment were also observed in the case of the SiO_2/SiC coaxial nanowires. Fig. 3 shows microscopy images of the pristine coaxial nanowires. They are mostly straight and have a consistent diameter along their length. Two coaxial samples were reacted at 5×10^{-5} mbar and 1450 °C, for 5 and 8 h, respectively. The two reacted samples were then subjected to local STEM based EELS line scans across the nanowires, compared to each other, and to pristine samples. This comparative study revealed some interesting differences.

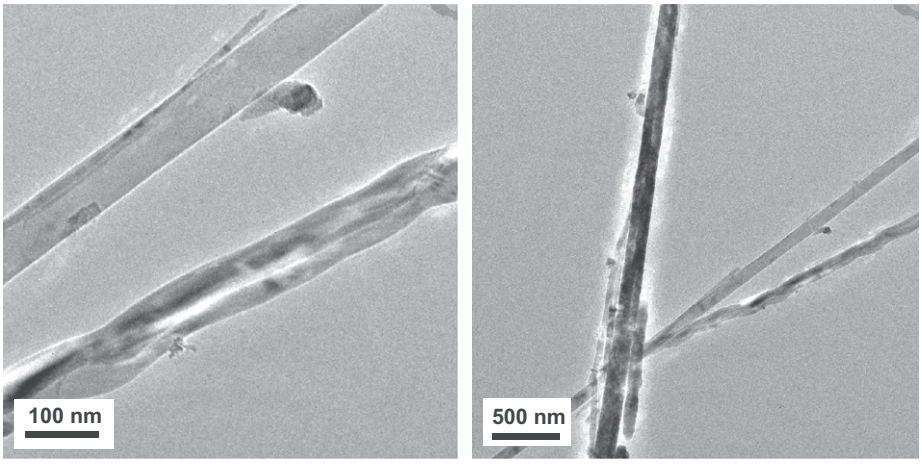

Fig. 3. TEM micrographs of the coaxial SiO_2/SiC nanowires used as starting material.

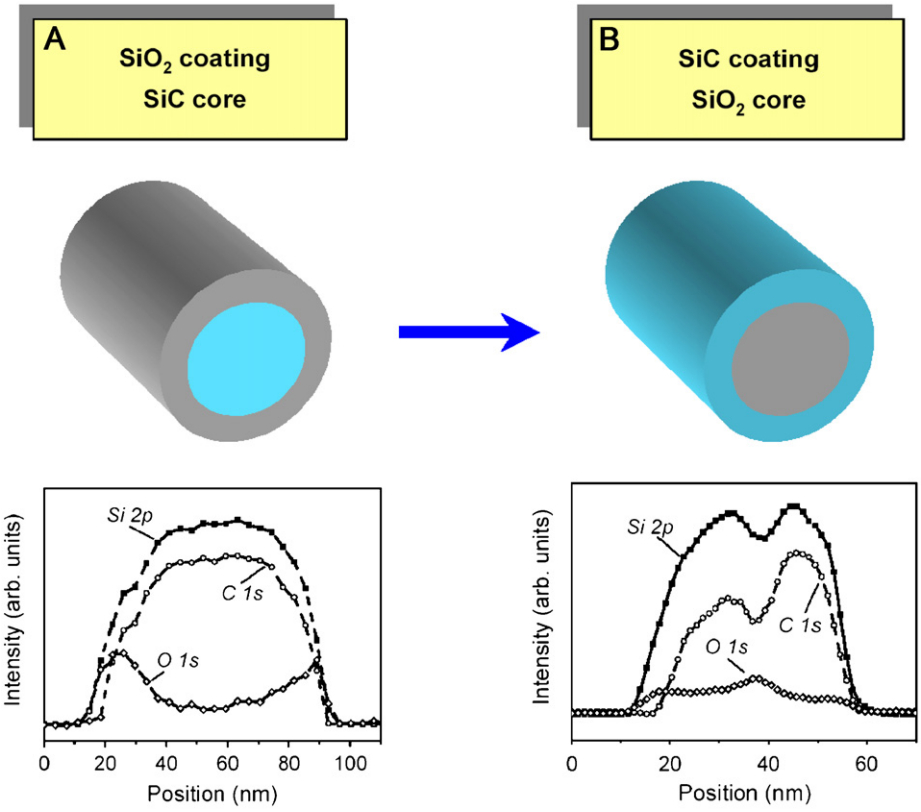

Scheme 2. Illustration of inter-conversion of nanowire cladding and core from (A) coaxial SiO_2/SiC nanowires to (B) coaxial SiC/SiO_2 nanowires. Lower panels show STEM based EELS line scans across each of the obtained nanostructures for the C1*s*, O1*s* and Si2*p* edges.

Line scans across the starting material show the pristine nanowires to have a thick SiC core and a thin SiO_2 coating (Scheme 2a). After 5 h treatment the Si and C profiles remain parabolic (as with the starting sample) but the O signal is now drastically diminished and spreads evenly across the nanowire. After 8 h annealing, the samples show distinct dips around the center of the nanowires whilst the O1*s* edge peaks at the center (Scheme 2b). Furthermore, the dip in the C edges of the measured nanorods was about 50% less than would be expected for SiC. This corresponds to an excess of Si at the center of the nanowires, which along with the presence of O_2 indicates the formation of SiO_2 at the center of the nanowires. Bulk EELS studies on these samples confirmed a bonding re-arrangement of the SiO_2 species [19]. The presence of SiC and SiO_2 throughout the various stages was also investigated using Raman and IR spectroscopy. Fig. 4 (left panel) shows the Raman spectrum for the various samples. All samples show a broad and asymmetric peak corresponding to SiC (cf. Fig. 2 left panel). Superimposed within the broad tail is a feature at ca. 820 cm^{-1}, which corresponds to a transverse and longitudinal optical pair (LO–TO) from crystalline SiO_2 [20]. This peak remains the same for all samples, both before and after the annealing reaction. In addition, a small peak just below 800 cm^{-1} is visible. This peak corresponds to the TO mode of SiC and is stronger for the post-annealed samples as compared to the raw sample (c.f. Fig. 2 left panel). This is in agreement with the previous results and again suggests the treatment improves the

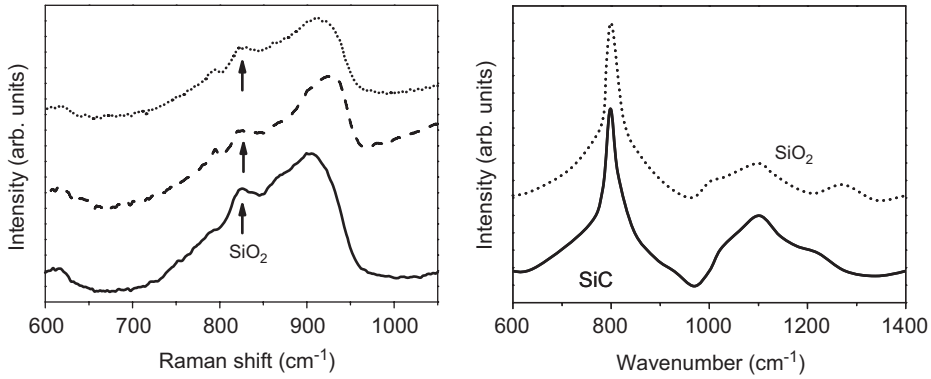

Fig. 4. Left panel: Raman spectra of the pristine coaxial SiO_2/SiC nanowires (full curve) and after two hydrogen thermal treatments; 5 h (dashed curve) and 8 h (dotted curve). Right panel: IR spectra of the pristine coaxial SiO_2/SiC nanowires (full curve) and 8h sample (dotted curve).

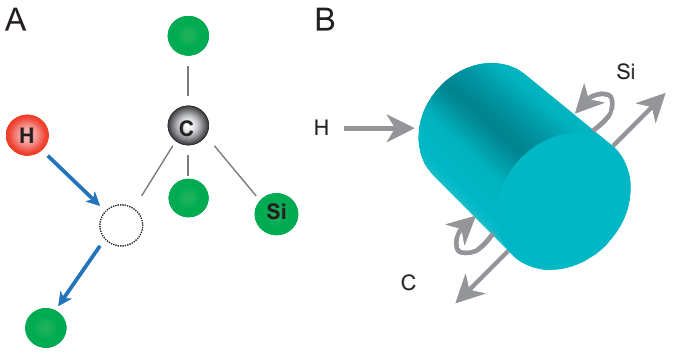

Scheme 3. (A) Schematic illustrating the substitution of Si by H in SiC. (B) Schematic showing the various diffusion pathways for the H, C and Si.

crystallization of the samples. The broad maxima around 940 cm^{-1} (SiC) is seen to slightly vary in position between samples. In Fig. 4 (right panel) the IR spectra for the pristine and 8 h reacted sample are presented. The IR spectrum of SiO_2 exhibits strong bands in between 1000 and 1300 cm^{-1}. In this region two split LO–TO pairs arising from Si–O asymmetric stretching are infrared active. At lower wavenumbers, ca. 800 cm^{-1}, the peak corresponding to SiC is clearly visible. No significant changes in the SiC peak between the pristine sample and 8 h reacted sample are observed. However, changes in the SiO_2 modes are clearly visible. The overall intensity of the bands relative to the SiC band is reduced in the 8 h reacted sample. This is consistent with the SiO_2 being at the core of the nanowires. Further, the band between 1200 and 1300 cm^{-1} is blue shifted in the 8 h reacted sample. The LO–TO splitting of the various SiO_2 modes has been shown to be dependant on heat treatment temperature [21] and so one might expect the heat treatment in our reaction to also affect the LO–TO splitting. This same argument can also explain the changes in the LO–TO splitting observed in the Raman spectra of these samples.

Notably, none of these samples exhibited any of these changes when pure nitrogen was used in place of hydrogen within the reaction. This observation implicates hydrogen as playing a key role in the observed morphology changes. It has been shown that H can displace Si in hydrogenated SiC and hydrogen preferentially bonds to C as opposed to Si [22]. This process leads to C–H bond formation in the structure. A preferential H substitution process in which Si is displaced and replaced by H is illustrated in Scheme 3a. C–H bonds break in the temperature range of 500–700 °C [23] and thus, in essence, the reaction leads to the decomposition of SiC. The substitution rate and hence decomposition will be greatest at the center of the nanowires as this is where the highest concentration of diffused hydrogen accumulates. This process provides a source of Si and C that can diffuse outward and reform on the outer surface of the nanostructures. The various diffusion routes are highlighted in Scheme 3b. This hydrogen activated process explains why the SiCNWs are converted to nanotubes and why they increase their diameters while doing so. Similar arguments can explain the inter-conversion of the coaxial nanowires. In this case, H also displaces the O in SiO_2. However, differences in diffusion rates and decomposition rates between the various species lead to the preferential accumulation of O toward the center of the nanowires enabling SiO_2 to form. This results in the inter-conversion of the coaxial structure of the SiO_2/SiCNWs.

4. Conclusions

Future and current technological demands for Si based nanostructures and films require a high degree of control in terms of etching, doping and structural manipulation. The presented annealing route using NH_3 as a hydrogen source is not only facile, but potentially can be applied to a variety of nanostructures and films pertinent to the semiconductor and composite industries, and beyond. These studies illustrate procedures to structurally modify or rearrange SiCNWs. Furthermore, the treatment improves the crystallization of the samples. Using our experimental methods, SiCNWs are shown to reform as nanotubes and coaxial SiO_2/SiCNWs are shown to reverse their core and coating. Our findings point to the preferential substitution by hydrogen and diffusion rates of species leading to the inter-conversion of species.

Acknowledgments

DFG PI 440-4 supported this work. Technical support from S. Leger and R. Hübel is gratefully acknowledged.

References

[1] J.R. Cooper, M.R. Melloch, R. Singh, A. Agarwal, J.W. Palmour, IEEE Trans. Electron Devices 49 (2002) 658–664.
[2] G.V. Soares, I.J.R. Baumvol, C. Radtke, F.C. Stedile, Appl. Phys. Lett. 90 (2007), 081906-1–081906-3.
[3] J. Kim, F. Ren, G.Y. Chung, M.F. MacMillan, A.G. Baca, R.D. Briggs, D. Schoenfeld, S.J. Pearton, Appl. Phys. Lett. 84 (2004) 371–373.
[4] D. Nakamura, I. Gunjishima, S. Yamaguchi, T. Ito, A. Okamoto, H. Kondo, S. Onda, H. Takatori, Nature 430 (2004) 1009–1012.
[5] Y. Ogura, T. Morimoto, J. Electrochem. Soc. 149 (2002) J47–J52.
[6] H.E. Eaton, G.D. Lindsey, J. Euro. Ceram. Soc. 22 (2002) 2741–2747.

[7] W.Q. Han, S.S. Fan, Q.Q. Li, B.L. Gu, D.P. Yu, Chem. Phys. Lett. 265 (1997) 374–378.
[8] G.Z. Shen, D. Chen, K.B. Tang, Y.T. Qain, S.Y. Zhang, Chem. Phys. Lett. 375 (2003) 177–184.
[9] A. Huczko, H. Lange, G. Chojecki, S. Cudziło, Y.Q. Zhu, H.W. Kroto, D.R.M. Walton, J. Phys. Chem. B 109 (2005) 16244–16251.
[10] G.W. Meng, L.D. Zhang, C.M. Mo, S.Y. Zhang, Y. Qin, S.P. Feng, J. Li, J. Mater. Res. 13 (1998) 2533–2538.
[11] N. Keller, C. Pham-Huu, G. Ehet, M.J. Ledoux, Carbon 41 (2003) 2131–2139.
[12] M.H. Rümmeli, E. Borowiak-Palen, T. Gemming, M. Knupfer, K. Biedermann, R.J. Kalenczuk, T. Pichler, Appl. Phys. A 80 (2005) 1653–1656.
[13] J. Fink, Adv. Electron. Electron Phys. 75 (1989) 121–232.
[14] Z. Deng, Z.S. Wu, J. Zhou, N.S. Xu, J. Chen, J. Chen, Chem. Phys. Lett. 356 (2002) 511–514.
[15] C. Pham-Huu, N. Keller, G. Ehret, M.J. Ledoux, J. Catal. 200 (2001) 400–410.
[16] T. Tomita, S. Saito, M. Baba, M. Hundhausen, T. Suemoto, S. Nakashima, Phys. Rev. B 62 (2000) 12896–12901.
[17] S. Nakashima, H. Harima, T. Tomita, T. Suemoto, Phys. Rev. B 62 (2000) 16605–16611.
[18] M. Hofmann, A. Zyweittz, K. Karch, F. Bechstedt, Phys. Rev. B 50 (1994) 13401–13411.
[19] M.H. Rümmeli, E. Borowiak-Palen, T. Gemming, A. Huczko, M. Knupfer, S. Cudzilo, R.J. Kalenczuk, T. Pichler, Synth. Met. 153 (2005) 349–352.
[20] P. González, J. Serra, S. Liste, S. Chiussi, B. León, M.P. Amor, J. Non-Cryst. Solids 320 (2003) 92–99.
[21] E.I. Kamitsos, A.P. Patsis, G. Kordas, Phys. Rev. B 48 (1993) 12499–12505.
[22] A.E. Kaloyeros, R.B. Rizk, J.B. Woodhouse, Phys. Rev. B 38 (1988) 13099–13106.
[23] H.Y. Wang, Y.Y. Wang, Q. Song, T.M. Wang, Mat. Lett. 35 (1998) 261–265.